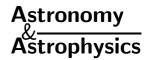
© ESO 2002



GHASP: An H α kinematic survey of spiral and irregular galaxies*,**

I. Velocity fields and rotation curves of 23 galaxies

O. Garrido, M. Marcelin, P. Amram, and J. Boulesteix

Observatoire Astronomique Marseille-Provence & Laboratoire d'Astrophysique de Marseille, 2 place Le Verrier, 13248 Marseille Cedex 04, France

Received 11 December 2001 / Accepted 1 March 2002

Abstract. GHASP (Gassendi H α survey of SPirals) is a survey of H α velocities in spiral and irregular galaxies. The observations began in 1998, with a scanning Fabry-Perot and a focal reducer attached at the Cassegrain focus of the 1.93 m telescope at the Observatoire de Haute-Provence. This paper presents the H α maps, the 2D velocity fields and the rotation curves obtained for a set of 23 galaxies observed in October 1998 and April 1999. Most of them have already been observed in HI in the frame of the WHISP survey led at Westerbork, for which GHASP brings an interesting complement. The aim is to provide a reference sample of 2D velocity fields for about 200 nearby spiral galaxies at H α wavelength.

Key words. galaxies: fundamental parameters – galaxies: kinematics and dynamics – galaxies: spiral – galaxies: irregular – galaxies: dwarf

1. Introduction

There are two main types of radial velocity measurements in galaxies, radio and optical ones. Radio observations give the velocity of neutral hydrogen, mainly with the 21 cm line, meanwhile optical observations give the velocity of ionized gas, mainly with $H\alpha$ and NII lines. Both techniques are complementary since radio observations enable one to reach the outermost parts of galaxies and optical observations provide a better spatial resolution (a few arcseconds instead of typically 10 to 30 arcsec). Most of the optical observations are based on slit spectroscopy, hence providing information along a single line, whereas Fabry-Perot technique allows one to obtain velocity measurements all over the observed galaxy, hence providing a complete 2D velocity field. This enables one to derive the true rotation curve, whereas in the case of slit spectroscopy it is often biased since the slit is oriented a priori along the position of the major axis determined from photometry observations, which is often off by several degrees from the kinematical major axis.

Despite this great advantage of the Fabry-Perot over the slit spectroscopy, most of the optical kinematical

Send offprint requests to: O. Garrido,

e-mail: olivia.garrido@observatoire.cnrs-mrs.fr

studies of galaxies are based on slit spectroscopy and generally limited to the analysis of the rotation curve. A large number of samples of rotation curves are available in the literature (e.g. Mathewson et al. 1992, with 965 H α rotation curves; Mathewson & Ford 1996, with $1051~\mathrm{H}\alpha$ rotation curves; Courteau 1997, with 304 galaxies; Dale et al. 1997, 1998 and 1999 with 522 rotation curves). However there is no large sample of 2D velocity fields at optical wavelengths, most of the Fabry-Perot observations being concerned with individual peculiar objects or small samples, observed at $H\alpha$ wavelength. The largest sample obtained up to now is that of 75 galaxies studied by Schommer et al. (1993) for measuring galaxy distances, followed by the sample of 45 galaxies obtained by Amram et al. (1995) for studying the behavior of galaxies in clusters. Let us mention also the sample of 7 galaxies observed by Beauvais & Bothun (1999) for studying noncircular motions, which is well suited for the Fabry-Perot since it is the only instrument capable of detecting small scale structures in the velocity fields because of both spatial and spectral resolution it offers.

By now, the total number of 2D velocity fields of galaxies available in the literature must be around two hundred, observed with various telescopes and different Fabry-Perot interferometers. The main reason is that the necessary exposure time is longer than with slit spectroscopy (typically 2h instead of 10 mn), another reason being that the Fabry-Perot technique is a bit more complicated for

 $^{^{\}star}$ Based on observations collected at the Observatoire de Haute de Provence.

^{**} All the figures are only available in electronic form at http://www.edpsciences.org

observing and for reducing data. This lack of a large homogeneous sample of 2D velocity fields of galaxies at optical wavelengths led us to initiate the GHASP project at the Observatoire de Haute-Provence. GHASP (acronym for Gassendi H α survey of SPirals) is a survey of galaxies led at Haute-Provence Observatory with a 1.93 m reflector equipped with a focal reducer and a Fabry-Perot interferometer. The aim is to obtain high resolution (both spatial and spectral) 2D velocity fields in the H α line of ionized hydrogen for about 200 nearby spiral and irregular galaxies. With this survey, we plan to complement the radio survey WHISP (Westerbork survey of HI in SPiral galaxies) led at Westerbork (Netherlands). Highresolution $H\alpha$ velocity fields are complementary to HI velocity fields mapping the outer galactic regions but suffering of beam-smearing and, most often, of a lack of emission in the inner parts. Began in 1993, WHISP is a survey of the neutral component in spiral and irregular galaxies with the Westerbork Synthesis Radio Telescope (WSRT) at 21 cm wavelength. Its aim is to obtain maps of the distribution and velocity structure of HI in 400 to 500 galaxies, increasing the number of well-analyzed HI observations of galaxies by an order of magnitude. The idea of its promoters is that such a uniform database will serve as a basis for research in many areas, for example: dark halos, effects of environment on the structure and growth of HI disks, and galaxy distances. More details can be found on the Web site http://www.astro.rug.nl/whisp/.

The GHASP survey will provide a homogeneous sample of 2D velocity fields which will cover a large range of luminosity and morphological types (except ellipticals) and will provide a complete reference sample at z=0. This sample will be used for comparison with galaxies observed: in various environments (pairs, groups, clusters); at different stages of evolution (mergers, starbursts) and at higher redshifts. The 2D velocity fields will be used to constrain the mass distribution of spirals, as explained in Sect. 6. Complementary photometric observations are in progress at the Observatoire de Haute-Provence to derive the distribution of dark matter in the galaxies of our sample. Also, we are going to compare our velocity fields with models in order to derive a theoretical interpretation (e.g. Amram 2002, for more informations).

2. The GHASP instrument

The GHASP instrument is attached at the Cassegrain focus of the 1.93 m telescope at the Observatoire de Haute-Provence. The original f/15 aperture ratio of the telescope is brought to f/3.9 through the focal reducer. The detector is a photon counting detector with 256×256 pixels, each pixel being 0.96 arcsec along each side, offering a field of view of about 4arcmin × 4 arcmin. Interference filters (typical FWHM .0 to 1.5 nm) enable one to select the H α line of ionized hydrogen (656.278 nm). This line, passing through the Fabry-Perot interferometer, finally produces interference rings. The pattern of the rings changes while the interferometer is scanned (the space between

the plates being changed by applying a precise voltage on piezoelectrics). Comparing the observed profiles with those given by a neon lamp used as a wavelength reference (659.895 nm) enables one to compute the wavelength shift through the Doppler effect, hence giving the radial velocity for each piece of ionized gas in the observed galaxy. The order of the Fabry-Perot used for GHASP is 798 at H α rest wavelength, giving a free spectral range of 376 km s^{-1} . Since we scan the interferometer through 24 channels the sampling step is about 15 km s⁻¹. However, the barycenter of the emission line profile may be measured with an accuracy much better than the sampling step, especially when the signal to noise is high (bright HII regions), hence giving a precision of about 5 km s^{-1} . Let us recall that the velocities measured with a Fabry-Perot are found modulo the free spectral range, which implies an a priori knowledge of the recession velocity of the observed galaxy (usually through slit spectroscopy or radio observation found in the literature) give or take the right number of free spectral ranges when computing the radial velocity.

The use of an IPCS (Image Photon Counting System) as a detector may seem surprising now that CCDs are the common standard, however it must be recalled that despite a smaller doe an IPCS has the great advantage of a zero readout noise. This makes such a device more powerful than CCDs for Fabry-Perot observations since it enables one to scan the interferometer as rapidly as we want (typically 10 s for each scanning step), reading and recording the images for each step (typically 24 steps), then scanning again the whole free spectral range and finally adding up the successive exposures for each scanning step when reducing the data. For a typical observation (2 hours exposure), the scanning sequence is repeated 30 times. This enables one to average the transparency conditions encountered along the exposure for each scanning step (this is especially true when there is a veil of cirrus clouds, but also when the sky is clear because of the change in airmass during the observation).

More details and illustrations can be found on the Web site http://www-obs.cnrs-mrs.fr/interferometrie/GHASP/ghasp.html

3. Observations and data reduction

The first observing run of GHASP took place in October 1998. Since then the runs take place every semester (typically 9 to 13 nights per run). We present here the results of the two first runs, representing 23 galaxies, all of which have been already observed by WHISP. Ten of them have been already studied by Swaters (1999) who used the WHISP data for obtaining the HI rotation curve. This enables a comparison with our H α rotation curves (for which we adopted the same inclination) commented in Sect. 5. Our first targets were mainly late-type dwarfs since the WHISP survey also began with this type of galaxies. For the following runs, we have observed other types of galaxies, trying to get a complete sample of all morphological types.

Table 1 gives the journal of the observations, with the following informations: Col. 1, name of the galaxy in the UGC catalog; Col. 2, name in the NGC catalog when available; Cols. 3 and 4, coordinates of the galaxy (equinox 2000); Cols. 5 and 6, central wavelength and *FWHM* of the interference filter used for the observation; Cols. 7 and 8, date of the observation and total exposure time in seconds.

The data reduction has been made with the software ADHOCw, written by J. Boulesteix, available on line at http://www-obs.cnrs-mrs.fr/adhoc/adhoc.html. The main lines of the data processing are the following:

- Adding and cleaning the original images (the photon counting detector records the individual frames, at a rate of 50 frames/s, the main correction to be applied is removing the detector remanence, which is done by comparing the successive frames).
- Computing the phase map from the calibration rings (schematically, this map gives the reference scanning channel to be used as wavelength origin for the line profile observed inside each pixel).
- Converting the observed interference patterns of a galaxy into "wavelength maps" by using the phase map. These maps are the optical equivalent of the "lambdamaps" produced in radio astronomy. They can be read directly as velocity slices, hence giving the velocity field of the galaxy. The substraction of nightskylines, such as OH emission lines, is generally made at this step of the data processing.
- Computing the velocity field, monochromatic and continuum maps. The velocity field is obtained by measuring the position of the barycenter of the $H\alpha$ line for each pixel. The monochromatic map is obtained by measuring the intensity found inside the line, above the local continuum. The continuum map is obtained by measuring the intensity found outside the emission line, it is in fact the small part of continuum emission from the galaxy passing through the interference filter. The crude data are smoothed in order to increase the signal to noise ratio in the faintest parts of the galaxy. A Gaussian smoothing is first applied on the $H\alpha$ profiles (with 3 channels FWHM) and another smoothing is applied spatially (in X and Y, with 3 pixels FWHM).
- Computing the rotation curve. The rotation curve is computed from the velocity field by taking into account the points found within a given angular sector from the major axis (in order to exclude the points too close to the minor axis for which the departure from pure circular motion is artificially exaggerated by the geometrical configuration, leading to a strong dispersion of the points on the rotation curve). We generally considered the points within \pm 50° from the major axis but sometimes restricted the sector to smaller values (especially for highly inclined galaxies). The other parameters to be adjusted for deriving the rotation curve are:
- Coordinates of the rotation center (ideally, it is the center of symmetry of the velocity field hence of the rotation curve, and we generally adopt the position of the

nucleus, as indicated by our continuum map, which is quite satisfactory in most cases; however, when no clear nucleus is found, we adopt the point giving the most symmetric rotation curve or appearing as the best center of symmetry for the isovelocity lines).

- Systemic velocity (recession velocity of the center of mass of the galaxy).
- Position Angle of the major axis (measured counterclockwise from the North, it may be quite different from the photometric major axis found in the literature, e.g. UGC 2455).
- Inclination of the disk with respect to the plane of the sky (0° for face on).

The set of parameters is adjusted through an iterative process minimizing the dispersion of the points along the rotation curve.

Typically the accuracy we obtained for these parameters is about 1 pixel (1 arcsec) for the position of the rotation center, 2 to 3 km s⁻¹ for the systemic velocity, 2 degrees for the PA of the major axis, but only 5 to 10 degrees for the inclination which is the less sensitive parameter.

Table 2 gives the values we found for the main kinematical parameters, together with some fundamental parameters found in the literature: Col. 1, name in UGC catalog; Col. 2, morphological type from NED; Col. 3, morphological type code t, from the LEDA data base; Col. 4, total apparent corrected B magnitude, $B^{\circ}T$, from LEDA; Col. 5, absolute B magnitude, M_b , from LEDA; Col. 6, systemic velocity deduced from our velocity field; Col. 7, distance D, deduced from the systemic velocity assuming $H_0 = 75 \text{ km s}^{-1} \text{ Mpc}^{-1}$; Col. 8, inclination deduced from the analysis of our velocity field, except for those already studied by Swaters (1999) in which case we adopted the same value for sake of homogeneity when making the comparison; Col. 9, position angle of the major axis deduced from our velocity field; Col. 10, total amplitude velocity, $\Delta V_{\rm max}$, observed on the rotation curve; Col. 11, maximum velocity, V_{max} , observed on the rotation curve; Cols. 12 and 13, outermost velocity point reached on the rotation curve, V_{last} and R_{last} being respectively the velocity and distance from the rotation center for this point; Col. 14, 1/2 S.A. is the half sector with respect to the major axis taken into account for computing the rotation curve.

About the systemic velocity, we note that the accuracy of the relative velocities measured inside a given galaxy is rather high (around 5 km s⁻¹ as explained in the previous section). However the absolute velocity itself is not so precise since the calibration is made with the neon line at 659.895 nm, while a galaxy is observed at the redshifted wavelength of the H α line. The problem is that the interferometer does not behave exactly the same in both cases since the coating layers behave differently depending on the wavelength (briefly things go as if the spacing between the plates of the interferometer changed between the calibration and the observation). The result is that our absolute velocities suffer from a systematic bias, negligible when the recession velocity is

Table 1. Log of the observations.

N° UGC	N° NGC	α (2000)	δ (2000)	λc	FWHM	date	exposure time (s)	
2034		$2^{\rm h}33^{\rm m}42.9^{\rm s}$	40°31′41″	6575.5 Å	11 Å	October, 15 1998	10 200	
2080		$2^{\rm h}36^{\rm m}27.9^{\rm s}$	$38^{\circ}58'12''$	6586	11.2	October, 13, 16 1998	22080	
2455	1156	$2^{\rm h}59^{\rm m}42.6^{\rm s}$	$25^{\circ}14'15''$	6575.5	11	October, 14 1998	3840	
2800		$3^{\rm h}40^{\rm m}3.3^{\rm s}$	$71^{\circ}24'21''$	6586	11.2	October, 15 1998	8640	
3574		$6^{\rm h}53^{\rm m}10.6^{\rm s}$	$57^{\circ}10'39''$	6596	10.3	October, 11, 12 1998	9360	
4325	2552	$8^{\rm h}19^{\rm m}20.1^{\rm s}$	$50^{\circ}00'25''$	6567	11.9	April, 4 1999	6240	
4499		$8^{\rm h}37^{\rm m}41.4^{\rm s}$	$51^{\circ}39'08''$	6576.5	11	April, 5 1999	10800	
5253	2985	$9^{\rm h}50^{\rm m}21.8^{\rm s}$	$72^{\circ}16'48''$	6597	10.3	April, 3 1999	10320	
5316	3027	$9^{\rm h}55^{\rm m}40.4^{\rm s}$	$72^{\circ}12'13''$	6587	11.2	April, 2 1999	7200	
5721	3274	$10^{\rm h}32^{\rm m}17.1^{\rm s}$	$27^{\circ}40'07''$	6576.5	11	April, 7 1999	8160	
5789	3319	$10^{\rm h}39^{\rm m}9.8^{\rm s}$	$41^{\circ}41'16''$	6576.5	11	April, 9 1999	6300	
5829		$10^{\rm h}42^{\rm m}42.2^{\rm s}$	$34^{\circ}26'56''$	6576.5	11	April, 10 1999	11760	
5931	3395	$10^{\rm h}49^{\rm m}50.1^{\rm s}$	$32^{\circ}58'59''$	6597	10.3	April, 11 1999	10800	
5935	3396	$10^{\rm h}49^{\rm m}55.2^{\rm s}$	$32^{\circ}59'27''$	6597	10.3	April, 11 1999	10800	
5982	3430	$10^{\rm h}52^{\rm m}11.9^{\rm s}$	$32^{\circ}57'06''$	6597	10.3	April, 8 1999	10080	
6778	3893	$11^{\rm h}48^{\rm m}38.2^{\rm s}$	$48^{\circ}42'40''$	6587	11.2	April, 7 1999	10080	
7524	4395	$12^{\rm h}25^{\rm m}48.9^{\rm s}$	$33^{\circ}32'48''$	6576.5	11	April, 12 1999	8640	
7971	4707	$12^{\rm h}48^{\rm m}22.9^{\rm s}$	$51^{\circ}09'53''$	6575	13.7	April, 6 1999	13920	
8490	5204	$13^{\rm h}29^{\rm m}36.5^{\rm s}$	$58^{\circ}25'09''$	6567	11.9	April, 3 1999	16020	
9969	5985	$15^{\rm h}39^{\rm m}37.1^{\rm s}$	$59^{\circ}19'55''$	6616.5	10.9	April, 10 1999	10440	
				6621.2	8.4	March, 11 2000	8400	
10310		$16^{\rm h}16^{\rm m}18.3^{\rm s}$	$47^{\circ}02'47''$	6576.5	11	April, 7, 8 1999	12340	
12060		$22^{\rm h}30^{\rm m}34^{\rm s}$	$33^{\circ}49'11''$	6586	11.2	October, 13, 14 1998	13920	
12754	7741	$23^{\rm h}43^{\rm m}53.9^{\rm s}$	$26^{\circ}04^{\prime}34^{\prime\prime}$	6566	11.9	October, 15 1998	10800	

close to 1650 km s⁻¹ (then the H α emission line of the galaxy is in coincidence with the neon line used for the calibration) but increasing with the departure from the calibration wavelength, reaching minus 10 km s⁻¹ for recession velocities around 0 km s⁻¹ and, symmetrically, plus 10 km s^{-1} for velocities around 3300 km s⁻¹. Correcting this bias, although theoretically possible (see pages 153 to 155 in Le Coarer's thesis, 1992), is not straightforward and the systemic velocities given in Table 2 are not corrected. Anyway, for the sample presented here, the average difference between our systemic velocities and that found on the Nasa Extragalactic Database is only -7 km s^{-1} with a dispersion of 9 km $\rm s^{-1}$ (taking into account 21 galaxies and excluding the pair UGC 5931 - UGC 5935 for which only the average velocity is given in the NED). This result seems quite acceptable, all the more since people are mainly interested in the relative velocities inside a galaxy, for which no correction is necessary.

N.B. Illustrations of the data processing can be found on the Web site http://www-obs.cnrs-mrs.fr/interferometrie/GHASP/ghaspdatareduction.html

4. Reduced H α data

For each galaxy we give the results of the data reduction in Figs. 1 to 22 (N.B.: UGC 5931 and UGC 5935 are on the same figure), with three frames per figure:

a. DSS image of the galaxy $(4' \times 4')$.

b. Isovelocity lines superimposed on the $H\alpha$ image of the galaxy (a colour coded version of the velocity field is available on the Web site of GHASP). These lines were drawn from the original velocity field (giving the heliocentric radial velocities) after a strong Gaussian smoothing (7 pixels FWHM), sometimes reiterated when the coverage of the galaxy by HII regions is faint, so as to obtain continuous lines. At some places with poor $H\alpha$ emission the continuity of the lines was artificially achieved by eye estimate and a dashed line plotted on the velocity field. In the worst cases, with only a few HII regions measured in a galaxy, it was impossible to draw any isovelocity line, then we directly wrote the average velocity value found for each HII region on the map . The H α image is derived from the analysis of the H α line profiles, by measuring the flux found inside the line for each pixel. It gives a pure monochromatic image of the galaxy. The intensity is coded here through gray levels (N.B. We have only relative intensity levels but no absolute calibration). Note that the $H\alpha$ images are sometimes markedly offset with respect to the DSS images. This is the case when we had to shift a bright star out of the field to prevent any damage to the photocathode of the IPCS but also when we offcentered the galaxy in order to prevent parasitic reflections inside the instrument (between Fabry-Perot plates and interference filter) from contaminating other parts of the galaxy. It must be noted also that in some cases, when the velocity amplitude is high and the interference filter is not

centered on the systemic velocity, one side of the galaxy is better transmitted than the other side, leading to an artificial asymmetry in the intensity of the H α emission. In some extreme cases (for instance UGC 9969) we had to observe the galaxy twice, with two different filters, one best suited for the redshifted side and the other one best suited for the blueshifted side.

c. Rotation curve of the galaxy. The rotation curve is drawn as explained in the previous section. We plotted the curve with both sides in the same quadrant, using different symbols for the receding and approaching side (with respect to the center itself): crosses are for receding and dots for approaching. To compute the values of the velocity and the radius, we consider elliptical crowns with a width of 3 to 6 pixels ($\sim 3''$ to 6'') and we thus obtain a middle velocity and radius for each crown. The choice of the width of the crowns depends on the quality of the data and on the extension of the curve. We decided to show the rotation curve since it is easy to derive from the velocity field and is commonly used for kinematical analysis, but it is clear that it offers a restricted view of the kinematics of a galaxy. A more complete analysis of the 2D velocity fields will be made in subsequent papers.

5. Comments on the observed galaxies

UGC 2034

This magellanic irregular exhibits a low velocity range (less than 60 km s⁻¹). The rotation curve is perturbated. No clear nucleus can be seen, so that the rotation center was found by symmetrizing at best the rotation curve. Despite the large dispersion, the agreement with the HI rotation curve of Swaters (1999) is quite satisfactory, but our H α curve hardly reaches 1 arcmin while the HI curve reaches 2 arcmin. Note however that the WHISP data show HI deficiency in the center.

UGC 2080

This late type spiral has a regular symmetric velocity field. Its rotation curve rapidly reaches a plateau around 280 km s⁻¹. The WHISP data show a faint HI column density (about half the typical value) with a well marked hole in the center.

UGC 2455 (NGC 1156)

This magellanic galaxy has two huge HII regions; one is found at about 20 arcsec south-west from the center and the other one at the very center. This last one has been spectroscopically analyzed by Ho et al. (1995) who showed that it is a Wolf-Rayet type source and concluded that this galaxy recently experienced a stellar burst (less than one million years ago). The velocity range is very low (less than 30 km s⁻¹ in radial velocity) and it is hard to derive a reliable rotation curve for this galaxy. Anyway the difference between the kinematical major axis and the photometric major axis, about 60° , is large enough to be significant. This discrepancy is also seen on the WHISP data which otherwise suggest a warp of

the disk, especially on the blueshifted side. Despite the large dispersion of our rotation curve, the agreement with the HI rotation curve of Swaters (1999) is acceptable. Let us note that, in the same manner as for UGC 2034, our $H\alpha$ curve barely reaches 1 arcmin meanwhile the HI curve extends up to 2 arcmin. Note also that the outermost receding points on our curve come from a single isolated region with an apparently anomalous behavior resulting in a lower than expected rotation velocity.

UGC 2800

This magellanic galaxy has poor H α emission and none in the central parts. Furthermore, it has a fairly regular and symmetric rotation curve, with a plateau at about 80 km s⁻¹. The WHISP data show that the HI emission is rather faint and asymmetric.

UGC 3574

The spiral structure is hardly seen on the H α image. The northern part is peppered with diffuse HII regions, meanwhile the southern part is dominated by three bright HII complexes. Nevertheless the rotation curve is fairly symmetric, reaching a plateau around 140 km s⁻¹. The WHISP data show HI deficiency in the center.

UGC 4325 (NGC 2552)

This magellanic galaxy exhibits a bright HII complex close to the center and two chains of bright HII regions looking like spiral arms. The rotation curve is mainly traced by the approaching points in the central part and by the receding points beyond 40 arcsec. The outermost point (approaching) is quite isolated, but suggests that the curve reaches a plateau around 90 km s⁻¹. Our rotation curve is in good agreement with the HI curve of Swaters (1999) but, again, does not go as far out. Note that the WHISP data indicate a high HI column density (about twice the typical value).

UGC 4499

This late magellanic galaxy has no clear nucleus (the rotation center was found by symmetrizing the rotation curve). The H α emission is asymmetric, with faint HII regions in the northern part and two extended complexes in the southern part, with one being remarkably huge (about 20 arcsec diameter, which is about 850 pc at the distance of UGC 4499) and bright. The rotation curve is quite symmetric, with a low gradient in the central part and reaches a plateau around 70 km s⁻¹. The comparison with the HI rotation curve of Swaters (1999) shows a significant offset, our curve being systematically higher by about 10 km s⁻¹ up to the plateau where both join. This discrepancy is probably due to an undercorrection of the beam smearing effect.

UGC 5253 (NGC 2985)

The H α emission in this early type galaxy is almost uniformly distributed in a ringlike structure, between 6 arcsec and 40 arcsec from the nucleus, with no emission

Table 2. Galaxy parameters.

N° UGC	Туре	t	$B^{\circ}T$ (mag)	M_b (mag)	$V_{\rm sys} \atop \rm (km\ s^{-1})$	D (Mpc)	i $(^{\circ})$	PA cor	$\Delta V_{ m max}$	$V_{\rm max} \ ({\rm km\ s}^{-1})$	$V_{\rm last} \ ({\rm km\ s}^{-1})$	$R_{ m last}$ (")	1/2 S.A.(°)
2034	${ m Im}$	9.7	12.9	-17.0	572 ± 1	7.6	19	162 ± 2	111	58	-61.4	-58	45
2080	SAB(rs)cd	5.9	11.2	-19.5	895 ± 0.5	11.9	10	155 ± 1	600	312	271.6	126.4	50
2455	IB(s)m	9.8	11.6		375 ± 0.5	5	51	105 ± 2	74	34.6	-33.8	-59	40
2800	${ m Im}$	9.9			1185 ± 1	15.8	50	100 ± 2	195	109	82	53	50
3574	SA(s)cd	5.8	14.1	-17.6	1435 ± 1	19.1	30	285 ± 3	318	161	-120	-107.3	50
4325	SA(s)m	8.9	12.1	-17.7	503 ± 1	6.7	41	229 ± 1	211	112	-82.7	-93.1	50
4499	SABdm	7.8	14.1	-16.2	680 ± 1	9.1	50	332 ± 2	153	78.8	-76.4	-88.7	40
5253	SA(rs)ab	2.3	10.8	-20.8	1320 ± 1	17.6	40	177 ± 2	515	261.8	-261.8	-92	50
5316	SB(rs)d	6.4	11.5	-19.7	1033 ± 1	13.8	70	302 ± 2	263	164.7	153.8	156.5	50
5721	SABd	6.6	12.6	-16.9	530 ± 1	7.1	61	102 ± 1	192	98.7	98.7	73.5	50
5789	SB(rs)cd	5.9	11.2	-19.2	730 ± 1	9.7	65	219 ± 1	242	130	130.3	179.4	50
5829	${ m Im}$	9.6	12.9	-17.1	628 ± 1	8.3	34	14 ± 1	96	56.6	-28.4	-158.9	50
5931	SAB(rs)	5.8	11.7	-20.1	1605 ± 1	21.4	50	182 ± 2	372	198	-198	-82	73
	cdpec												
5935	IBmpec	9.4	11.5	-20.3	1678 ± 1	22.4	70	72 ± 2	121	65.9	-51.4	-27.1	40
5982	SAB(rs)c	5.1	11.5	-20.3	1569 ± 1	21	60	212 ± 1	445	222.3	-223.2	-141.4	50
6778	SAB(rs)c	5.1	10.4	-20.6	958 ± 1	12.8	30	167 ± 1	593.5	305	295.4	968	50
7524	SA(s)m	8.7	10.6	-17.3	318 ± 2	4.2	46	147 ± 2	142	73.9	-62.5	-185.9	50
7971	Sm	8.7	13.1		463 ± 1	6.2	38	215 ± 2	60	32.8	27.3	49.8	50
8490	SA(s)m	8.8	11.1	-17.7	191 ± 1	2.6	50	357 ± 2	175	95.2	74.8	124.1	50
9969	SAB(r)b	3.0	11.2	-21.7	2520 ± 1	33.6	60	197 ± 2	663	363.6	261.8	130.8	60
10310	SB(s)m	9.2	13.1	-17.4	705 ± 1	9.4	34	27 ± 2	169	83	68.5	62	40
12060	Ibm	9.8	14.8	-16.0	892 ± 1	11.9	40	15 ± 2	192	114.2	-103.6	-119.5	50
12754	SB(s)cd	5.9	11.5	-18.9	742 ± 1	9.9	45	162 ± 2	270	136.7	127.5	111.8	50

at all in the center and faint emission in the spiral arms around the ring. The isovelocity lines are fairly symmetric, with classical distortions when crossing the spiral arms. The velocity gradient in the center is very high and the rotation curve rapidly reaches a plateau at $240~\rm km~s^{-1}$. The WHISP data indicate a faint HI column density in the main body and a large off-centered ring, about 16 arcsec in diameter.

UGC 5316 (NGC 3027)

This barred galaxy is strongly asymmetric, with only one well marked spiral arm in the visible and $H\alpha$ wavelengths on one side of the galaxy, while the other side is much more extended in HI, as can be seen on the WHISP data. The rotation curve is fairly symmetric and exhibits a solid body rotation shape up to the outermost point reached in our data (about 2.5 arcmin from center).

UGC 5721 (NGC 3274)

This irregular galaxy has an elongated main body with very bright HII regions making a bar-like structure. Another chain of regions, to the east, looks like a second bar roughly parallel to the main one; meanwhile another chain of regions looks like a spiral arm to the west. In the central parts the isovelocity lines are almost parallel and aligned along the main body, as observed in regular barred galaxies. The shape of the velocity lines suggests a warp of the disk, confirmed by the WHISP velocity field. As a result, the PA of the major axis changes significantly

between the center (where it is about 125°) and the outer parts (where it is about 95°). We adopted the intermediate value 100° for tracing the rotation curve, which reaches a sort of a plateau around 80 km s^{-1} . The agreement with the HI rotation curve of Swaters (1999) is very good but we reach the plateau at about 1 arcmin from the center whereas the HI curve extends up to 4 arcmin.

UGC 5789 (NGC 3319)

This barred galaxy has an asymmetric distribution of $H\alpha$ emission, the northern spiral arm and the bar being rather poor whereas the southern arm exhibits bright HII regions. The rotation curve is fairly symmetric, slowly climbing with a solid body shape up to about 2 arcmin from the center, where it reaches a maximum around 100 km s⁻¹. The same behavior can be seen on the WHISP data. Our better spatial resolution enables one to see a pause in the climbing part of the curve, at about 40 arcsec from the center, marking the end of the bar. Martin & Friedly (1997) have studied the morphology of this bar and concluded that it is young (less than 1 Gyr).

UGC 5829

This odd galaxy has no clear shape. The velocity amplitude is small, about 50 km s^{-1} , the slope of the rotation curve is very faint and a plateau seems to be reached at about 1.1 arcmin from the center (at least for the blueshifted side, because the redshifted side is

not entirely in our field). The same tendency can be seen on the WHISP data, despite the strong deficiency of HI emission in the central part. The HI emission is mainly concentrated on the eastern side of the galaxy, along a north-south aligned structure coinciding with a chain of HII regions which dominates our H α image. The HI rotation curve of Swaters (1999) does not go further out than our H α curve but shows a continuous climb and, except close to the center, is systematically above our curve by 10 to 20 km s⁻¹, suggesting a possible overcorrection of the beam smearing effect.

UGC 5931 (NGC 3395)

This late type spiral is interacting with a smaller galaxy, UGC 5935, as can be seen in the kinematics. Indeed the velocity field of UGC 5931 shows strong distortions, clearly due to the interaction. A large HII complex lying between the two galaxies most probably belongs to the main galaxy as suggested by the continuity of the velocities. Despite the velocity field distortions, making it hard to find the kinematical major axis, the rotation curve appears fairly symmetric. It reaches a local maximum, around 100 km s⁻¹, at the end of the main body, between 30 and 40 arcsec from the center, then declines slightly before climbing again beyond 1 arcmin from the center, up to 200 km s^{-1} . The climbing part corresponds to the large HII complex mentioned hereabove for the redshifted side and to a seemingly secondary spiral arm towards the SW for the blueshifted side. Both structures have a symmetric behavior and their velocities suggest a motion departing from a pure rotation in the main plane of the galaxy. They are maybe about to separate from the main body because of the interaction. The WHISP HI data show an extended S shaped structure around the optical body, probably corresponding to large tidal tails, especially to the south where it covers more than 10 arcmin.

UGC 5935 (NGC 3396)

This companion of UGC 5931 is strongly affected by the interaction with the main galaxy as shown by its rotation curve, clearly more asymmetric than that of UGC 5931. The redshifted side exhibits a solid body rotation, meanwhile the blueshifted side remains almost flat up to 15 arcsec, before climbing with about the same slope as the redshifted side. The WHISP HI data have no sufficient spatial resolution to permit any kinematical study of this object. Moreover it seems much poorer in HI than the main galaxy.

UGC 5982 (NGC 3430)

This galaxy has a strange spiral pattern, with 3 arms, seen in visible light as well as in $H\alpha$. In fact it seems that there is a secondary western arm, parallel to the main one. Despite its oddity this galaxy has a regular velocity field, with classical wiggles at the crossing of the main spiral arms. Its rotation curve is quite typical of its type, rapidly reaching a plateau around 180 km s⁻¹.

Both sides are perfectly symmetric. The rising part at the end of the curve, seen on the blueshifted side, could be explained by the interaction with UGC 5972. The WHISP HI data clearly suffer from a technical problem since almost no signal was detected (see graphical overview on their Web site) whereas Nordgren et al. (1997) have observed it with the VLA successfully when studying its interaction with its neighbour UGC 5972. They show that the disks of both galaxies are warped at the outer edges and that there is a tidal tail extending from UGC 5982 towards the NE, also they underline that the optical images show little sign of tidal interaction.

UGC 6778 (NGC 3893)

This late type spiral exhibits a regular velocity field with wiggles at the crossing of the spiral arms. The rotation curve is fairly symmetric, slowly rising up to 1 arcmin from the center, where it reaches a plateau at about 280 km s⁻¹. A pause can be seen in the rising part, at about 20 arcsec from the center, marking the end of the small central bar (one can see also the typical alignment of the velocity lines along the bar). The WHISP HI data suggest that the rotation curve gets down beyond 2 arcmin but the H α emission is not enough extended to check that. However the beginning of the strong warp seen on the WHISP velocity field can be seen on the redshifted side of our data. This warp is probably due to the interaction with UGC 6781, 4 arcmin towards the SE, both galaxies appearing connected through a long HI tail.

UGC 7524 (NGC 4395)

This magellanic galaxy is a Seyfert 1 type. It is quite near and thus only the central part can be seen in the GHASP field of view, with huge HII regions in the southeastern part. The slope of the rotation curve is very slow, with a decreasing part at about 1 arcmin from the center, especially well marked on the redshifted side, and no plateau is being reached within 3 arcmin from the center. Indeed, the WHISP HI data even suggest that the rotation curve is still rising at 8 arcmin from the center, at least for the redshifted side.

UGC 7971 (NGC 4707)

The H α emission of this magellanic spiral is concentrated in a few bright HII regions at the periphery of the main body. It is thus impossible to draw a velocity field and we just give the approximate velocity values for the 5 brighter HII regions, from which one can hardly guess the position of the major axis. The derived rotation curve is not very significant because of the paucity of the H α emission. The WHISP HI data show a large HI hole in the center of the galaxy, the HI gas appearing as a ring surrounding the main optical body. The WHISP HI velocity field suggests a solid body rotation with a small amplitude, as confirmed by the HI rotation curve derived by Swaters (1999). No clear comparison with our H α curve is possible because of the high dispersion of our points. Indeed, the low values of the rotation velocities we

find in the outer parts, on the receding side, are produced by two HII regions only, the motions of which may not be representative at all of the average motion in the disk.

UGC 8490 (NGC 5204)

This galaxy has a mottled appearance and the spiral structure is hard to see. The variations in the isovelocity lines, together with the distribution of HII regions, suggest the presence of a central ring, about 30 arcsec in radius. The rotation curve is fairly symmetric, gently rising up to about 80 km s⁻¹ at the limit of our H α data, at 2 arcmin from the center (the higher points, on the redshifted side, are not significant because they come from a single isolated region). The WHISP HI data indicate that we are then reaching the maximum of the curve, they also show that the disk is strongly warped beyond the optical limits. This warp can be partly seen in our data, for the blueshifted side only because of insufficient data on the other side. The HI rotation curve derived by Swaters (1999) is systematically found 10 km s^{-1} above our $H\alpha$ curve in the rising part, suggesting a possible overcorrection of the beam smearing effect.

UGC 9969 (NGC 5985)

The large velocity amplitude of this spiral (almost 700 km s^{-1}) obliged us to observe it twice, with two different interference filters, since we had no filter well suited to get both sides of the galaxy in a single exposure. The galaxy has two main arms, one splitting into two parts to the west, and the isovelocity lines show classical variations at the crossing of the spiral arms. The rotation curve is fairly symmetric, reaching a plateau around 300 km s⁻¹, at about 50 arcsec from the center. The blueshifted side is clearly more perturbed than the redshifted side for which the curve is much more regular and the plateau perfectly flat. However, since the observations were made in two steps and both sides observed with different filters and different sky conditions, this may be due to a difference in quality of the observations and is not intrinsic to the galaxy. The WHISP HI data show that the HI emission is rather faint and confined within a ring surrounding the main optical body, about 2 arcmin in radius.

UGC 10310

This magellanic barred spiral has rather poor $H\alpha$ emission, but exhibits a very bright giant HII region to the SE. Some emission can be seen in the north part of the bar and in the spiral arms starting at both ends. The scarcity of the emission makes the drawing of isovelocity lines difficult. It is also hard to derive a reliable rotation curve, although both sides are in fairly good agreement and suggest that a maximum around 70 km s⁻¹ is reached at about 50 arcsec from the center. The WHISP HI data show that the neutral gas is mainly concentrated in the two spiral arms. Our $H\alpha$ velocities are consistent with the HI velocity field, as confirmed by the good agreement between our rotation curve and the HI curve derived by Swaters (1999).

UGC 12060

This magellanic barred spiral has rather poor ${\rm H}\alpha$ emission outside the bar itself. Here again it is hard to draw isovelocity lines and in many cases we could only write directly on the map the velocity measured for isolated regions. Despite the high dispersion of the velocities and the lack of data on the redshifted side, the rotation curve is quite acceptable, with a plateau around 100 km s⁻¹ reached at about 1.5 arcmin from the center. This behavior, rather surprising for a magellanic type galaxy, is confirmed by the WHISP HI data. However, the HI rotation curve derived by Swaters (1999) has a plateau below 80 km s⁻¹ meanwhile its rising part is slightly above our ${\rm H}\alpha$ curve, suggesting a possible overcorrection of the beam smearing effect in the rising part.

UGC 12754 (NGC 7741)

This late-type barred spiral has a prominent bar and two short spiral arms. There are bright HII regions in the bar and arms but the H α emission appears quite mottled all over the disk. A detailed study of its HII regions and $H\alpha$ velocity field has been made by Duval et al. (1991). The rotation curve is fairly symmetric and in very good agreement with that of Duval et al., reaching a plateau around 130 km $\rm s^{-1}$ at about 1.2 arcmin from the center. Also, the same decrease in the curve can be seen on both approaching and receding sides, between 30 and 40 arcsec, which precisely marks the end of the bar. The WHISP HI data show that the HI emission is almost restricted to the optical disk, so that the position-velocity diagram does not bring more information than the H α data beyond 2 arcmin. It suggests however that the rotation curve is slightly decreasing in the outer parts, the maximum being reached around 1.5 arcmin from the center. The shape of our plateau also suggests the same tendency, for both redshifted and blueshifted sides.

6. Discussion

The rotation curves of galaxies provide useful information on the distribution of gravitational matter. In this respect, they are crucial for the study of dark matter. Both HI and $H\alpha$ data are needed to draw conclusions about the presence of cusped haloes, about the quantity of dark matter and the availability of the hypothesis of maximum disk, in a spiral galaxy (e.g. Evans 2001). Because of beam smearing effects, the HI rotation curves seem to have gentler slopes than those obtained with $H\alpha$ data, which makes wrong the determination of the density of dark haloes in the inner parts of the galaxies (particularly for the LSB disks and dwarf spirals). Evans concludes that "only when the HI data is complemented by $H\alpha$ observations can robust conclusions be drawn".

Blais-Ouellette et al. (1999, 2001, 2002) have shown that both the dark and luminous components are very sensitive to the rising part of the rotation curve, that it is very difficult to correct the radio data for the beam smearing effect and that the Fabry-Perot is to be preferred to long slit spectroscopy to derive properly the orientation parameters. They conclude that the optimal rotation curve is clearly a combination of 2D high resolution spectroscopy for the inner part of spiral galaxies and high sensitivity radio observations for the outer regions. The comparison made in Sect. 5 between H α rotation curves and HI rotation curves (Swaters 1999) for ten galaxies, shows that there is a good agreement for 5 out of 10 galaxies, the HI curve is found slightly above the H α curve for 2 galaxies and more clearly above for 2 others meanwhile it is clearly below for another one. On average it appears that there is a slight tendency to overcorrection. On a larger sample of 19 late-type dwarfs, Amram & Garrido (2002) found that the HI rotation curves corrected for beam smearing effects do not agree with the high resolution curves obtained with hybrid $H\alpha/HI$ data (they also found that the disk M/L computed from the HI rotation curve is greater than that computed from the hybrid rotation curve for two thirds of this sample of 19 galaxies). This confirms that the beam smearing correction done on the HI data is on average too strong.

Besides the catalogue aspect of the GHASP survey, it also enables detailed studies of individual galaxies. A good example is provided by the study of ram pressure stripping in NGC 4522, in Virgo, by Vollmer et al. (2000). The survey is still ongoing and the sample increasing regularly. By now, about 120 galaxies have been observed and the data analysis is in progress. This survey, once completed, will provide a 3-D sample of 200 nearby spiral and irregular galaxies in the $H\alpha$ line, using a Fabry-Perot. The data cubes obtained for each galaxy allow us to deriv line maps and velocity fields. The main goals of this survey are: (1) To build a 3D local reference sample. (2) To constrain the mass distribution. (3) To constrain the kinematics and dynamics of the internal regions. A data base will be built in order to provide the complete data to the community.

Acknowledgements. The authors thank J. L. Gach and O. Boissin for their help when preparing the instrument. They are grateful to Stéphane Xavier for his contribution to the data reduction. They also thank the Groupement de Recherche Galaxies for its support for observing time and the Observatoire de Haute-Provence team for its technical

assistance during the observations. The authors wish to thank the anonymous referee who helped improving the manuscript.

References

Amram, P., & Garrido, O. 2002, Galaxies: the third dimension, ed. M. Rosado, L. Binette, & L. Arias [astro-ph/0202475]
Amram, P., Boulesteix, J., Marcelin, M., et al. 1995, A&ASS, 113, 35

Beauvais, C., & Bothun, G. 1999, ApJS, 125, 99

Blais-Ouellette, S. 2002, Galaxies: the third dimension, ed. M. Rosado, L. Binette, & L. Arias

Blais-Ouellette, S., Carignan, C., & Amram, P. 2001, AJ, 121, 1952

Blais-Ouellette, S., Carignan, C., Amram, P., & Côté, S. 1999, AJ, 118, 2123

Courteau, S. 1997, AJ, 114, 2402

Dale, D. A., Giovanelli, R., Haynes, M. P., et al. 1997, AJ, 114, 455

Dale, D. A., Giovanelli, R., Haynes, M. P., et al. 1998, AJ, 115, 418

Dale, D. A., Giovanelli, R., Haynes, M. P., et al. 1999, AJ, 118, 1468

Duval, M. F., Monnet, G., Boulesteix, J., et al. 1991, A&A, 241, 375

Evans, N. W. 2001, invited review for IDM 2000: Third International Workshop on the Identification of Dark Matter, ed. N. Spooner (World Scientific) [astro-ph/0102082]

Ho, L. C., Filippenko, A. V., & Sargent, W. L. W. 1995, ApJS, 97, 477

Le Coarer, E. 1992, Thèse de doctorat de l'Université Paris 7 Mathewson, D. S., & Ford, L. 1996, ApJS, 107, 97

Mathewson, D. S., Ford, L., & Buchhorn, M. 1992, ApJ, 389, 5

Martin, P., & Friedly, D. 1997 A&A, 326, 449

Nordgren, T. E., Chengalur, J. N., Salpeter, E. E, & Terzian, Y. 1997 AJ, 114, 77

Schommer, R. A., Bothun, G. D., Williams, T. B., & Mould, J. R. 1993, AJ, 105, 97

Swaters, R. A. 1999 Dark matter in late-type dwarf galaxies, Thesis, Rijksuniversiteit Groningen

http://www.ub.rug.nl/eldoc/dis/science/r.a.swaters/Vollmer, B., Marcelin, M., Amram, P., et al. 2000, A&A, 364, 532